

Research Article

Jiachen Luo, Zongliang Du*, Yilin Guo, Chang Liu, Weisheng Zhang and Xu Guo*

Multi-class, multi-functional design of photonic topological insulators by rational symmetry-indicators engineering

<https://doi.org/10.1515/nanoph-2021-0433>

Received August 8, 2021; accepted September 28, 2021;

published online October 13, 2021

Abstract: An explicit topology optimization-based design paradigm is proposed for the design of photonic topological crystalline insulators (TCIs). To strictly guarantee the topological property, rational engineering of symmetry-indicators is carried out by mathematical programming, which simultaneously maximizes the width of nontrivial topological band gaps and achieves the desired quantized bulk polarization. Our approach is successfully applied to design photonic TCIs with time-reversal symmetry in two-dimensional point groups, higher-order magnetic TCIs, and higher-order photonic TCIs. This methodology paves the way for inverse design of optimized photonic/phononic, multiphysics, and multifunctional three-dimensional TCIs.

Keywords: higher-order topological insulator; symmetry-indicator; topological crystalline insulator; topological insulator; topology optimization.

1 Introduction

Topological insulators (TIs), as a new class of materials, have a unique ability to protect energy propagation against various defects, and thus have a great potential in applications of different fields [1–3]. From theoretical aspects, it has been well-recognized that symmetry is highly related to the topological property of TIs. Specifically, Fu et al.

first proposed eigenvalues of parity (the primitive form of symmetry-indicators [SIs]) to classify nontrivial TIs from ordinary materials with inversion symmetry [4]. Later on, Schnyder et al. generalized this classification method by incorporating more intrinsic symmetries, such as the time-reversal symmetry (TRS) [5].

In 2011, Fu proposed a new type of TIs – topological crystalline insulators (TCIs), whose topological property can be selectively protected by the crystallographic symmetry of lattice [6]. The rich variety of crystalline symmetries in solids provides an enormous potential to realize TCIs. Later on, Fang et al. and Benalcazar et al. simplified the formulation of bulk polarization and further efficiently identified a number of nontrivial TCIs by using eigenvalues of crystallographic point group operators [7, 8] (i.e., the generalized SIs from the well-known parity index in [4]). Notably, only eigenvalues of symmetry operation at the high-symmetry momenta are necessary for the SIs-based classification scheme, which has been successfully applied for the whole 230 space groups [9, 10], the whole 1651 magnetic space groups [11], and recently identified thousands of new TIs, TCIs, and semimetals [12, 13].

Following the development of TIs in the Fermion system, next, the TIs in the photonic and phononic systems attracted much attention as well [14–22]. To circumvent the computational burden of repeatedly calculating topological invariants such as Chern number, alternative inverse design methodologies have been proposed for photonic and phononic TIs. For instance, the topologically protected propagation path or the desired band structures of spin-Hall and higher-order topological insulators (HOTIs) are designed by structural topology optimization [23–29]. By realizing the band inversion phenomena and maximizing the working bandwidth of topological edge state, a pair of optimized acoustic valley-Hall insulators, and more recently photonic/phononic valley/spin-Hall TIs were obtained [30, 31]. Nevertheless, most of the above works take a post-procedure to verify the topological invariant of optimized designs, nor constraining the topological invariant during the optimization process. Therefore, it is

*Corresponding authors: Zongliang Du and Xu Guo, State Key Laboratory of Structural Analysis for Industrial Equipment, Department of Engineering Mechanics, Dalian University of Technology, Dalian, China, E-mail: zldu@dlut.edu.cn (Z. Du), guoxu@dlut.edu.cn (X. Guo). <https://orcid.org/0000-0002-5924-438X> (Z. Du)

Jiachen Luo, Yilin Guo, Chang Liu and Weisheng Zhang, State Key Laboratory of Structural Analysis for Industrial Equipment, Department of Engineering Mechanics, Dalian University of Technology, Dalian, China

still a challenge to guarantee the topological property of intermediate designs. At this circumstance, it would be interesting and instructive to rationally design photonic and phononic TIs with certain topological properties based on the efficient calculation of topological invariant by taking the advantages of SIs [7, 13].

In this work, we propose a systematic inverse design method for the two-dimensional (2D) spinless TCIs through engineering the SIs, and then generalize it for HOTIs. First, a brief introduction to SIs and a general mathematical formulation for obtaining TCIs in 2D point groups are proposed. Then the validity of the design paradigm is demonstrated by the rational design of photonic TCIs with TRS, HOTI with magnetic material, and multiphysics HOTI.

2 Identification of nontrivial TCIs using SIs

Topological invariants, e.g., the Chern number, which corresponds to the integration of Berry curvature in the whole Brillouin zone, are the essential factors to identify nontrivial TIs from ordinary materials. As refer to works [4, 7], the Chern number can also be determined by the inversion eigenvalues at high-symmetry points (i.e., the SIs). Particularly, in the present work, such as TCIs with TRS, the Chern number always vanishes, and the relation between the Chern number and SIs becomes a trivial identity. At this circumstance, some new topological invariants, e.g.,

the bulk polarization, are desired [7, 8]. According to Fang's work [7], in 2D case, the bulk polarization is effective for TCIs and it is defined as

$$\mathbf{P} = P_1 \mathbf{a}_1 + P_2 \mathbf{a}_2 \quad (1)$$

with $\mathbf{a}_{i=1,2}$ denoting the lattice vectors, and its components are

$$P_i = -\frac{1}{2\pi} \int_0^1 dk_1 \int_0^1 dk_2 \text{Tr}(\mathcal{A}_i(k_1 \mathbf{b}_1 + k_2 \mathbf{b}_2)) \quad (2)$$


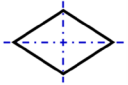
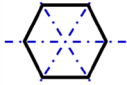
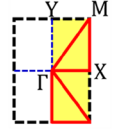
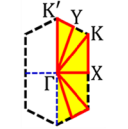
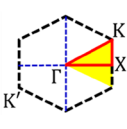
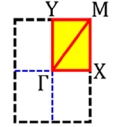
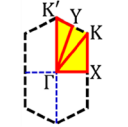
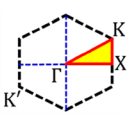
where $k_{j=1,2}$ are the components of wave vector and $\mathbf{b}_{j=1,2}$ are the reciprocal lattice vectors, and the Berry connection $\mathcal{A}_{i=1,2}$ are defined using the Bloch function \mathbf{u} as $[\mathcal{A}_i]_{jl} = -i \langle \mathbf{u}_j | \partial_{k_i} | \mathbf{u}_l \rangle$.

For the m th band, define the corresponding SIs as the eigenvalues ξ^m of the symmetry operator \hat{C} at high-symmetry momenta \mathbf{k}_{inv} , i.e., $\hat{C} |\mathbf{u}^m(\mathbf{k}_{\text{inv}})\rangle = \xi^m |\mathbf{u}^m(\mathbf{k}_{\text{inv}})\rangle$, where the high symmetry momentum is identified by $\hat{C} \mathbf{k}_{\text{inv}} = \mathbf{k}_{\text{inv}}$ modulo a reciprocal lattice vector. For 2D cyclic point groups C_n and dihedral point groups C_{nv} ($n = 2, 3, 4, 6$), denoting ζ^m and θ^m as the SIs of \hat{C}_2 and \hat{C}_3 operators, respectively, the corresponding components of bulk polarization are simplified as [7, 8]

$$e^{i2\pi P_i} = \prod_m \delta_i^m \quad (3)$$

The relations between δ_i^m and ζ^m, θ^m as well as the nontrivial quantized bulk polarizations are presented in Table 1 for the considered 2D lattices.

Table 1: The bulk polarization in 2D point groups for TCIs (For $n = 6$, its bulk polarization always vanishes [7, 8]).

	$n = 2$	$n = 3$	$n = 4$
Lattices with C_n or C_{nv} symmetry			
First Brillouin zone of C_n lattices with reduced zone colored in yellow			
First Brillouin zone of C_{nv} lattices with high-symmetry lines colored in red			
Bulk polarization (P_1, P_2)	$\delta_1^m = \frac{\zeta^m(X)}{\zeta^m(\Gamma)}, \delta_2^m = \frac{\zeta^m(Y)}{\zeta^m(\Gamma)}$	$\delta_1^m = \delta_2^m = \frac{\theta^m(K)}{\theta^m(\Gamma)}$	$\delta_1^m = \delta_2^m = \frac{\zeta^m(X)}{\zeta^m(\Gamma)}$
Non-trivial (P_1, P_2) for C_n	$(\frac{1}{2}, 0), (0, \frac{1}{2}), (\frac{1}{2}, \frac{1}{2})$	$(\frac{1}{3}, \frac{1}{3}), (\frac{2}{3}, \frac{2}{3})$	$(\frac{1}{2}, \frac{1}{2})$
Non-trivial (P_1, P_2) for C_{nv}	$(\frac{1}{2}, 0), (0, \frac{1}{2}), (\frac{1}{2}, \frac{1}{2})$	$(\frac{1}{2}, \frac{1}{2})$	

3 SI-based optimization formulations of TCIs

3.1 Description of lattice using explicit topology optimization method

In the photonic and phononic systems, properties of lattice can be artificially modulated by designing the material distribution inside, for instance, using structural topology optimization. In the Moving Morphable Components (MMC) method [32, 33], the target material distribution is obtained by optimizing the locations, shapes and sizes of a set of components. For lattices with specific symmetries, as shown in Figure 1, the design variables only contain the geometry parameters of the components in the reduced lattice as $\mathbf{D} = (x_0^{[j]}, y_0^{[j]}, \rho^{[j]}, \phi^{[j]})^T$, where $x_0^{[j]}$ and $y_0^{[j]}$ are the coordinates of center of the j th component; $\rho^{[j]} = \{\rho_s^{[j]}\}$ is the length vector of all control lines $\{\text{OP}_s\}$ of the j th component; $\phi^{[j]}$ is the rotation angle of the j th component. More details can be found in Refs. [30, 31, 33].

3.2 Mathematical formulation

Based on the SI-aided calculation of bulk polarization and the explicit geometry description of lattices, an optimization formulation for the nontrivial phononic or photonic TCIs with maximized width of bandgap is proposed:

$$\begin{aligned} &\text{Find} && \mathbf{D} \\ &\text{Max.} && \min_{\mathbf{k}} f_{\mathbf{k}}^{m+1} - \max_{\mathbf{k}} f_{\mathbf{k}}^m \\ &\text{S.t.} && \nabla^2 \Psi + k_0^2 \Psi = \mathbf{0} \\ &&& H(P_1, P_2) = 0 \end{aligned} \quad (4)$$

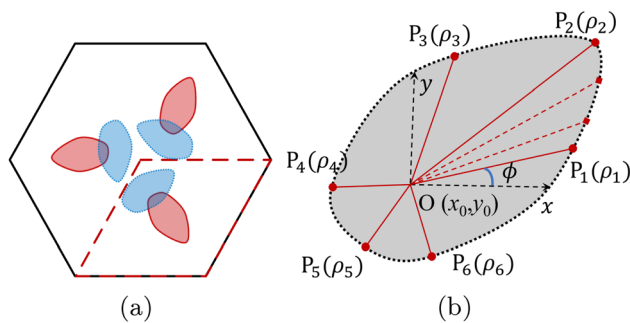


Figure 1: An illustration of a photonic or phononic lattice described by the MMC method. (a) A C_3 -symmetric hexagonal lattice described by two components (the reduced lattice is boxed in red-dashed lines), (b) geometry parameters for the adopted component.

where \mathbf{D} is the design variable of lattice described by the MMC method; the objective function is the width of m th bandgap with $f_{\mathbf{k}}^m$ denoting the eigenfrequency (normalized by the lattice constant A and the velocity of base medium c) of the m th band at the wave vector \mathbf{k} . The first constraint is the general time-independent wave equation and k_0 denotes the wavenumber. The SI-related constraint $H(P_1, P_2)$ is an exact adjustment of the bulk polarization according to the desired topological property. To be specific, for the case when either the P_1 or P_2 is nonzero, it implies the existence of a nontrivial edge state; when both the P_1 and P_2 are nonzero, it corresponds to a HOTI with topological corner states; however, when both the P_1 and P_2 are zero, one needs further advanced verification to identify its topological property [8, 13], and it is out of the scope of this work. The concrete form of the SI-related constraint will be elaborated in the forthcoming applications.

4 Applications

4.1 Inverse design of optimized photonic TCIs

In general, to guarantee the nontrivial property of the TCIs, for diamond lattice with C_{2v} -symmetry, the constraint function $H(P_1, P_2)$ is given as

$$H(P_1, P_2) = \text{sign}(P_1 \cdot P_2) - 1 \quad (5)$$

while for the rest symmetry cases in Table 1 (For the case of $n = 3, 4$, Eq. (5) is also applicable), the above function could be¹

$$H(P_1, P_2) = \text{sign}(P_1 + P_2) - 1 \quad (6)$$

Setting the base medium as Vacuum (colored in green, $\epsilon_r^{\text{Vac}} = \mu_r^{\text{Vac}} = 1$) and the scattering medium as Silicon (colored in orange, $\epsilon_r^{\text{Si}} = 11.7$, $\mu_r^{\text{Si}} = 1$), by solving Eqs. (4) and (6), optimized TM photonic rectangular lattice with C_2 -symmetry is obtained as shown in Figure 2(a). The corresponding width of the 1st nontrivial normalized bandgap is about 0.113, which is much wider than the bandwidth of a reference design in literature [21]. In addition, the bulk polarization vector $(0, 1/2)$ implies the nontrivial topological property as well as a selective topological

¹ To produce optimized designs with a specific bulk polarization, e.g., $(1/2, 0)$, the SI-related constraint can be refined as $H(P_1, P_2) = \text{sign}(P_1 - P_2) - 1 = 0$.

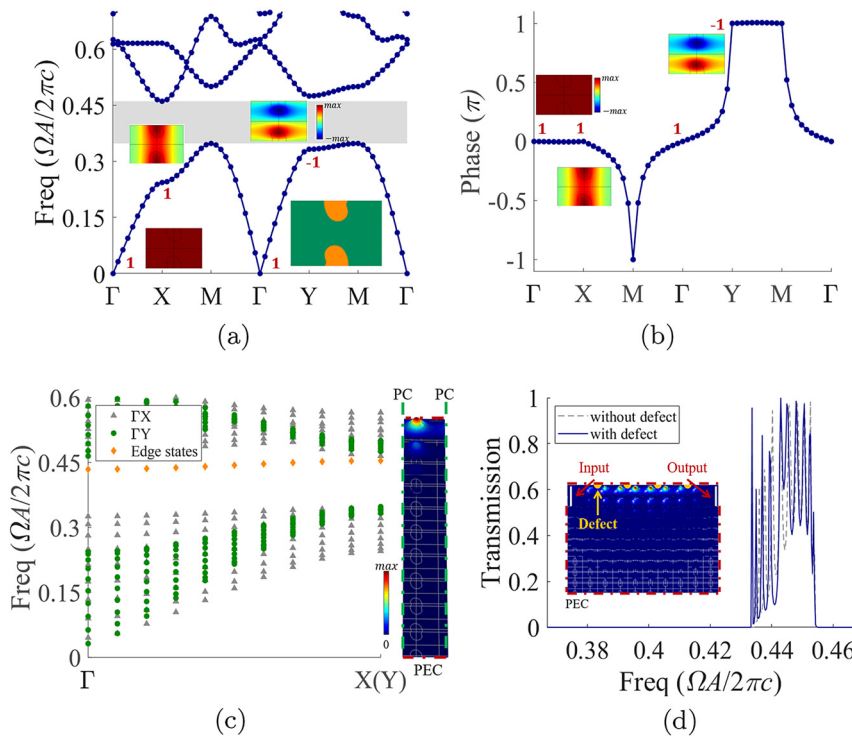


Figure 2: The optimized rectangular lattice with C_2 -symmetry. (a) The unit cell and its band structure. The inserted diagrams are the eigenstates at high-symmetry momenta, and markers “ ± 1 ” displayed their parities; (b) the phase diagram $\Phi_2^m(\mathbf{k})$ of the 1st band; (c) the supercell’s band along ΓX (gray-triangle point) and ΓY (green-circle point) with truncation (more detail of truncation refers to Appendix B), and edge state (along ΓX) denoted as a yellow-diamond point. The inserted eigenstate corresponds to the ΓX ’s edge state of Γ point; (d) the transmission spectrum of edge states without and with defects, where defects are denoted as yellow semi-circles in the inserted full-wave simulation result. Periodic condition is denoted as PC with green dashed line in Figure 2(c); all free boundaries (i.e., the red dash-dot lines unless otherwise stated) for TM wave are set as perfect electric conductor (PEC) in Figure 2(c) and (d).

edge state. This prediction is consistent with the parity of the eigenstates at high-symmetry momenta presented in Figure 2(a). Specifically, in Figure 2(b), the variations of a phase quantity [18] (i.e., $\Phi_2^m(\mathbf{k}) = -I \ln \zeta(\mathbf{k})$) illustrate an increment of π from 0 in the segment ΓY . And such phase difference is an intrinsic topological property of the optimized TCIs under the C_2 rotation operation. On the other hand, similar to the reported selectively protected edge state of TCIs [21], for the optimized design, there is only a highly localized edge state appearing in ΓX as the illustration in Figure 2(c). Notably, although the band structure of Figure 2(c) is not gapless, its nontrivial topological property is protected by the quantized bulk polarization [18, 19]. And this point is further demonstrated by the transmission spectrum of edge states without and with defects illustrated by Figure 2(d). These phenomena validate the engineered topological properties by bulk polarization.

Furthermore, nontrivial TCIs with other symmetries in Table 1 are also successfully obtained based on the proposed optimization formulation, as refer to Appendix A.

As revealed, a common feature of those nontrivial TCIs is that the scattering medium is mainly located at lattice’s corners or boundaries, not its center. This is determined by the constraint of nontrivial bulk polarization.

4.2 Inverse design of optimized higher-order topological gyromagnetic insulators

For the HOTIs, in 2D case, the novel feature is the topological corner state, which could be produced by polarization vectors with both nonzero components [34]. Consequently, the HOTIs could be obtained in the proposed design paradigm with constraint Eq. (5), such as the optimized C_{nv} -symmetric gyromagnetic HOTIs. For example, we set the base medium as Vacuum ($\epsilon_r^{\text{vac}} = \nu_r^{\text{vac}} = 1$, $\gamma_r^{\text{vac}} = 0$, colored in green of Figure 3(a)), and the scatterer is frequency-independent gyromagnetic material-YIG ($\epsilon_r^{\text{YIG}} = 15$, $\nu_r^{\text{YIG}} = 15$, $\gamma_r^{\text{YIG}} = 12.4$, colored in orange) with an anisotropic permeability

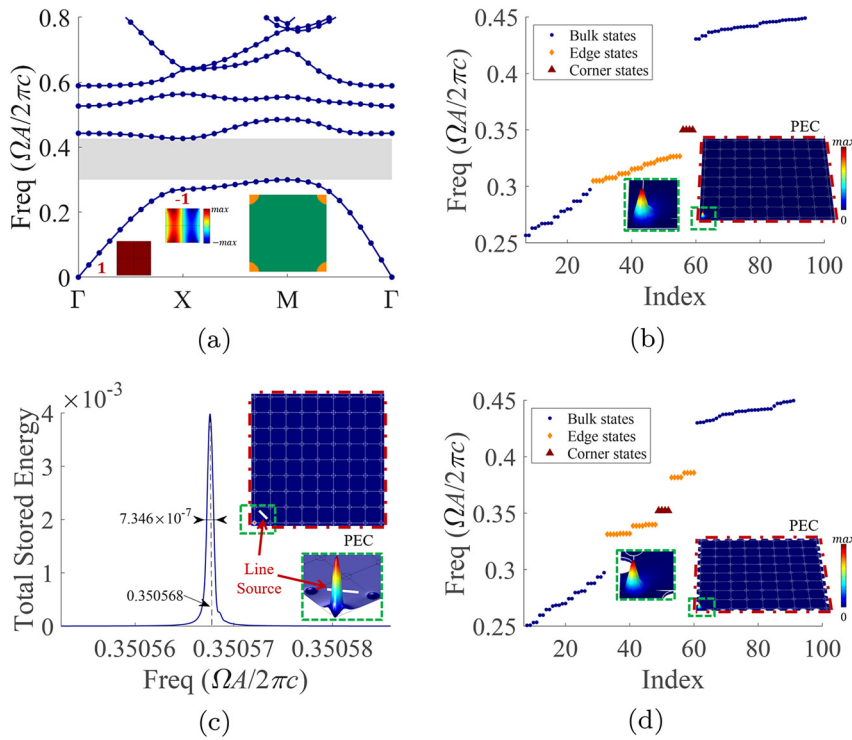


Figure 3: The optimized C_{4v} -symmetric gyromagnetic HOTI. (a) The unit cell and its band structure. The inserted diagrams and markers “ ± 1 ” displayed their parities at high-symmetry momenta; (b) the supercell’s spectrum and highly localized corner states with truncation, where the inserted red-triangle points reveal the corner states; (c) the spectrum of the stored energy of the corner states with the inserted diagrams illustrating the full-wave simulation result at the mid-frequency; (d) the spectrum and corner states of supercell after the perturbation about the cavity, denoted as a white semi-circle with radius 20% A .

$$\mu_r = \begin{bmatrix} v_r & I\gamma & 0 \\ -I\gamma & v_r & 0 \\ 0 & 0 & 1 \end{bmatrix} \quad (7)$$

The optimized square C_{4v} -symmetric gyromagnetic HOTI with bulk polarization of $(1/2, 1/2)$ and the 1-st bandgap of about 0.300–0.430 is shown in Figure 3(a). In Figure 3(b), the corresponding supercell displayed 4 corner states in its bulk gap (i.e., the red-triangle points) and they are all highly localized at corners, which have a Q-factor of about 477,000 illustrated in Figure 3(c) and the mode volume is less than $0.051A^2$. After a perturbation along its edges, the corner states still robustly locate in the bulk gap and keep localized energy, as shown in Figure 3(d) and Appendix B. This verifies the topological properties of the proposed gyromagnetic HOTI.

4.3 Inverse design of higher-order topological photonic insulators

The proposed design paradigm can also be applied to the topological multiphysics system, such as photonic HOTIs which are simultaneous nontrivial as photonic and

phononic materials. In order to preserve both highly localized corner states of photonics and phononics, the widths of nontrivial band gaps for both systems are maximized. The mathematical formulation for the photonic HOTIs with TRS is upgraded as:

$$\begin{aligned} & \text{Find} \quad \mathbf{D} \\ & \text{Max.} \quad \min \left\{ \min_k f_k^{\text{TM},m+1} - \max_k f_k^{\text{TM},m}, \right. \\ & \quad \left. \min_k f_k^{\text{Ac},m+1} - \max_k f_k^{\text{Ac},m} \right\} \quad (8) \\ & \text{S.t.} \quad \nabla^2 \mathbf{E}_z + k_0^2 \mathbf{E}_z = \mathbf{0} \\ & \quad \nabla^2 \mathbf{p} + \bar{k}_0^2 \mathbf{p} = \mathbf{0} \\ & \quad \text{sign}(P_1^{\text{TM}} \cdot P_2^{\text{TM}} \cdot P_1^{\text{Ac}} \cdot P_2^{\text{Ac}}) - 1 = 0 \end{aligned}$$

Here, \mathbf{E}_z is the z -component of the electric field in the TM system; \mathbf{p} is the pressure field in the acoustic system. The superscripts “TM” and “Ac” identify the parameters in photonics and phononics, respectively.

Setting the base medium as Air (colored in green, $\epsilon_r^{\text{Air}} = \mu_r^{\text{Air}} = 1$, $\rho^{\text{Air}} = 1.29 \text{ kg} \cdot \text{m}^{-3}$, $c_p^{\text{Air}} = 344 \text{ m} \cdot \text{s}^{-1}$) and the scattering medium as Silicon (colored in orange, $\epsilon_r^{\text{Si}} = 11.7$, $\mu_r^{\text{Si}} = 1$, $\rho^{\text{Si}} = 2329 \text{ kg} \cdot \text{m}^{-3}$, $c_p^{\text{Si}} = 5340 \text{ m} \cdot \text{s}^{-1}$), the optimized hexagonal photonic HOTI with C_3 -symmetry is obtained in Figure 4. As illustrated in Figure 4(a) and (b),

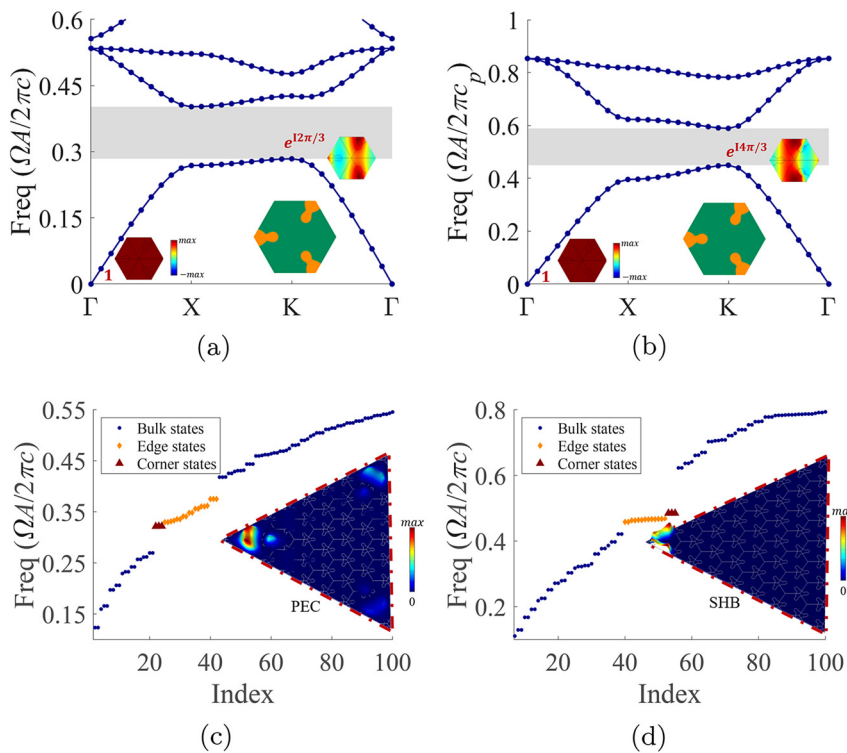


Figure 4: The optimized C_3 -symmetric photonic HOTI. (a) and (b) The unit cell and the photonic and phononic band structures with SIs illustrated by the inserted eigenstates; (c) and (d) the photonic and phononic spectrum and highly localized corner states with truncation. The inserted eigenstates illustrate their energy field of corner states. All free boundaries (the red dash-dot lines) for TM/acoustic wave are set as PEC/Sound hHard bBoundary (SHB) by default in this paper.

the quantized bulk polarizations in photonic and phononic systems are $(1/3, 1/3)$ and $(2/3, 2/3)$, and the corresponding nontrivial normalized band gaps locate at $0.284\text{--}0.402$ and $0.450\text{--}0.589$, respectively. The photonic and acoustic corner states of a triangular supercell as well as the corresponding spectrums are displayed in Figure 4(c) and (d). Interestingly, the vibrations are concentrated at different mediums, i.e., Silicon for photonics and Air for acoustics. This is consistent with the corresponding nontrivial bulk polarizations in photonics and acoustics. Furthermore, the appearance of such highly localized corner states in photonic system also offers a possibility of an efficient photon–phonon transducing [35, 36].

5 Summary

By taking the advantage of SIs in the efficient calculation of quantized bulk polarizations, an explicit structural topology optimization-based design framework is proposed for photonic and phononic TCIs with maximized width of nontrivial band gaps. The universality and effectiveness of the proposed design paradigm are verified from different

levels: (1) the first-order photonic TCIs with TRS among the 2D point groups; (2) the higher-order TCIs in magnetics, i.e., the gyromagnetic HOTIs; (3) the photonic HOTIs as a representative of multi-functional multiphysics TIs. Besides the rationality of mathematical programming about SIs successfully engineered the topological nontrivial phases, the optimized performances, such as the selective topological boundary states and a high Q-factor, are also significant in practical applications of topological devices. More interestingly, the proposed inverse design method could also be extended for three-dimensional topological materials and compatible with machine learning techniques [37, 38].

Author contribution: All the authors have accepted responsibility for the entire content of this submitted manuscript and approved submission.

Research funding: This work is supported by the National Natural Science Foundation (11821202, 11732004, 12002073, 12002077, 11922204, 11872141), the National Key Research and Development Plan (2020YFB1709401), the Fundamental Research Funds for the Central Universities (DUT20RC(3)020, DUT21RC(3)076), Dalian Talent Innovation Program (2020RQ099), Liaoning Revitalization

Talents Program (XLYC1907119), Doctoral Scientific Research Foundation of Liaoning Province (2021-BS-063) and 111 Project (B14013).

Conflict of interest statement: The authors declare no conflicts of interest regarding this article.

Appendix A: Optimal design of TCIs with TRS in the 2D point groups

Distributing one MMC in the reduced lattices belonging to the 2D point groups in Table 1, mathematical programming Eq. (4) for the 1-st band gap is solved individually using Genetic Algorithm (GA) in MATLAB and COMSOL, following the flowchart in Figure A1. Incorporating the SI-related constraint Eq. (5) for diamond lattices with C_{2v} -symmetry and Eq. (6) for the rest cases), the nontrivial TCIs with the considered symmetries and their bulk polarizations are presented in Table A1. The parameters adopted in GA are the population size of 50, the crossover fraction of 0.9, the migration fraction of 0.3, the elite count of 3, the stall generation limit of 15, and the fitness function tolerance of

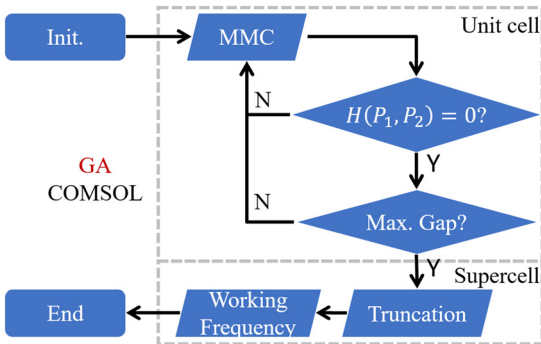


Figure A1: The flowchart for topology optimization of TCIs.

Table A1: Optimized TCIs with TRS among the 2D point groups in Table 1.

	n = 2				n = 3	n = 4
Lattice	Rectangular		Diamond		Hex	Square
C_n						
(P_1, P_2)	(0,1/2)	(1/2,1/2)	(0,1/2)	(1/2,1/2)	(1/3,1/3)	(1/2,1/2)
C_{nv}						
(P_1, P_2)	(1/2,0)	(1/2,1/2)		(1/2,1/2)	(2/3,2/3)	(1/2,1/2)

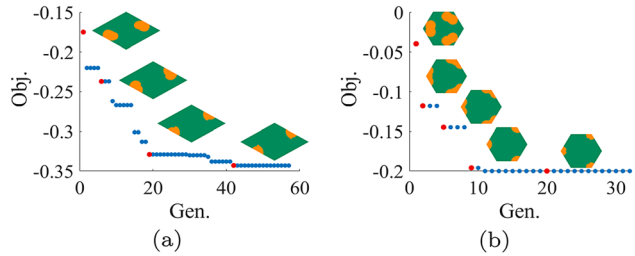


Figure A2: Iteration histories of the optimized diamond TCI with C_2 -symmetry and the optimized C_{3v} -symmetric hexagonal TCI.

10^{-5} . Some representative iteration histories of the design process are illustrated in Figure A2.

Appendix B: Adjustment of truncation for supercell's interface

As referred to in works [18–20], the quantized bulk polarization vector (P_1, P_2) is also called as the Wannier center. Any mismatch between the lattice's center and the Wannier center has a direct influence on the edge states and corner states. Specifically, this Wannier-type HOTI requires its supercell's edge should cut through the Wannier centers, otherwise the corner state is invisible. In comparison to this Wannier-type HOTI, the TCIs, topologically protected by their crystalline symmetries, are robust to external perturbation from the translation or rotation of boundaries [18, 34]. This implies it is not necessary for the supercell-boundary exactly cross the Wannier centers. Therefore, an additional adjustment of the edges of a supercell, i.e., a truncation $T = (T_1, T_2)$ as illustrated in Figure B1(a)–(c), is also introduced for producing more localized topological edge states and corner states. Figure B1(d) also makes a visible illustration for the corner states' topological properties in the perturbation of defects within the 2nd example.

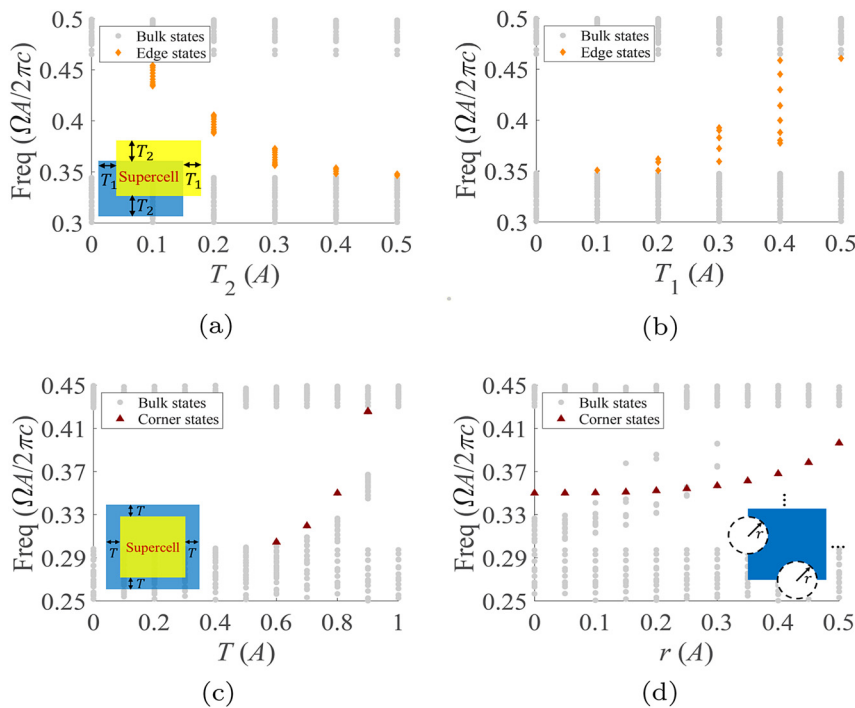


Figure B1: The effects of different truncations on supercell's projective band. For example 1, (a) the supercell's ΓX projective band under the truncation $T = (0, T_2)$, where the edge states are denoted as red-triangle points and the insert diagram is the illustration of the truncation treatment $T = (T_1, T_2)$; (b) the supercell's ΓY projective band under the truncation $T = (T_1, 0)$. For example 2, (c) the supercell's spectrum under the truncation $T = T_1 = T_2$ and (d) the evolution of corner states with respect to vacuum defects (circle defects with radio radius r in four boundaries). Here, the corner states are denoted as red-triangle points.

It should be pointed out that, the truncation is only applied to the edges of the supercell composed of the optimized lattice with maximized width of the nontrivial bandgap. This adjustment could be treated as a kind of defect, and it would not sacrifice the topological property of obtained TCIs.

References

- [1] L. Lu, J. D. Joannopoulos, and M. Soljačić, "Topological photonics," *Nat. Photonics*, vol. 8, no. 11, pp. 821–829, 2014.
- [2] S. Oh, "The complete quantum Hall trio," *Science*, vol. 340, no. 6129, pp. 153–154, 2013.
- [3] C. Felser and X. L. Qi, "Topological insulators," *MRS Bull.*, vol. 39, no. 10, pp. 843–846, 2014.
- [4] L. Fu, C. L. Kane, and E. J. Mele, "Topological insulators in three dimensions," *Phys. Rev. Lett.*, vol. 98, no. 10, p. 106803, 2007.
- [5] A. P. Schnyder, S. Ryu, A. Furusaki, and A. W. W. Ludwig, "Classification of topological insulators and superconductors in three spatial dimensions," *Phys. Rev. B*, vol. 78, no. 19, p. 195125, 2008.
- [6] L. Fu, "Topological crystalline insulators," *Phys. Rev. Lett.*, vol. 106, no. 10, p. 106802, 2011.
- [7] C. Fang, M. J. Gilbert, and B. A. Bernevig, "Bulk topological invariants in noninteracting point group symmetric insulators," *Phys. Rev. B*, vol. 86, no. 11, p. 115112, 2012.
- [8] W. A. Benalcazar, T. Li, and T. L. Hughes, "Quantization of fractional corner charge in Cn-symmetric higher-order topological crystalline insulators," *Phys. Rev. B*, vol. 99, no. 24, p. 245151, 2019.
- [9] H. C. Po, A. Vishwanath, and H. Watanabe, "Symmetry-based indicators of band topology in the 230 space groups," *Nat. Commun.*, vol. 8, no. 1, pp. 1–9, 2017.
- [10] B. Barry, L. Elcoro, J. Cano, et al., "Topological quantum chemistry," *Nature*, vol. 547, no. 7663, pp. 298–305, 2017.
- [11] H. Watanabe, H. C. Po, and A. Vishwanath, "Structure and topology of band structures in the 1651 magnetic space groups," *Sci. Adv.*, vol. 4, no. 8, p. eaat8685, 2018.
- [12] F. Tang, H. C. Po, A. Vishwanath, and X. Wan, "Topological materials discovery by large-order symmetry indicators," *Sci. Adv.*, vol. 5, no. 3, p. eaau8725, 2019.
- [13] F. Tang, H. C. Po, A. Vishwanath, and X. Wan, "Efficient topological materials discovery using symmetry indicators," *Nat. Phys.*, vol. 15, no. 5, pp. 470–476, 2019.
- [14] L. H. Wu and X. Hu, "Scheme for achieving a topological photonic crystal by using dielectric material," *Phys. Rev. Lett.*, vol. 114, no. 22, p. 223901, 2015.
- [15] Z. Zhang, Qi. Wei, Y. Cheng, T. Zhang, D. Wu, and X. Liu, "Topological creation of acoustic pseudospin multipoles in a flow-free symmetry-broken metamaterial lattice," *Phys. Rev. Lett.*, vol. 118, no. 8, p. 084303, 2017.
- [16] T. Ma and G. Shvets, "All-Si valley-Hall photonic topological insulator," *New J. Phys.*, vol. 18, no. 2, 2016, Art no. 025012.

- [17] X. Zhang, H. X. Wang, Z. K. Lin, et al., “Second-order topology and multidimensional topological transitions in sonic crystals,” *Nat. Phys.*, vol. 15, no. 6, pp. 582–588, 2019.
- [18] X. Ni, M. Weiner, A. Alu, and A. B. Khanikaev, “Observation of higher-order topological acoustic states protected by generalized chiral symmetry,” *Nat. Mater.*, vol. 18, no. 2, pp. 113–120, 2019.
- [19] Q. Wu, H. Chen, X. Li, and G. Huang, “In-plane second-order topologically protected states in elastic Kagome lattices,” *Phys. Rev. Appl.*, vol. 14, no. 1, p. 014084, 2020.
- [20] M. Ezawa, “Higher-order topological insulators and semimetals on the breathing Kagome and pyrochlore lattices,” *Phys. Rev. Lett.*, vol. 120, no. 2, p. 026801, 2018.
- [21] Bi. Ye. Xie, H. F. Wang, H. X. Wang, et al., “Second-order photonic topological insulator with corner states,” *Phys. Rev. B*, vol. 98, no. 20, p. 205147, 2018.
- [22] H. Chen, H. Zhang, Q. Wu, et al., “Creating synthetic spaces for higher-order topological sound transport,” *Nat. Commun.*, vol. 12, no. 1, pp. 1–10, 2021.
- [23] R. E. Christiansen, F. Wang, and O. Sigmund, “Topological insulators by topology optimization,” *Phys. Rev. Lett.*, vol. 122, no. 23, p. 234502, 2019.
- [24] R. E. Christiansen, F. Wang, O. Sigmund, and S. Stobbe, “Designing photonic topological insulators with quantum-spin-Hall edge states using topology optimization,” *Nanophotonics*, vol. 8, no. 8, pp. 1363–1369, 2019.
- [25] Y. Chen, F. Meng, B. Jia, G. Li, and X. Huang, “Inverse design of photonic topological insulators with extra-wide bandgaps,” *Phys. Status Solidi Rapid Res. Lett.*, vol. 13, no. 9, p. 1900175, 2019.
- [26] H. W. Dong, S. D. Zhao, R. Zhu, Y. S. Wang, L. Cheng, and C. Zhang, “Customizing acoustic Dirac cones and topological insulators in square lattices by topology optimization,” *J. Sound Vib.*, vol. 493, p. 115687, 2021.
- [27] S. S. Nanthakumar, X. Zhuang, H. S. Park, C. Nguyen, Y. Chen, and T. Rabczuk, “Inverse design of quantum spin Hall-based phononic topological insulators,” *J. Mech. Phys. Solid.*, vol. 125, pp. 550–571, 2019.
- [28] Y. Chen, F. Meng, Y. Kivshar, B. Jia, and X. Huang, “Inverse design of higher-order photonic topological insulators,” *Phys. Rev. Res.*, vol. 2, no. 2, p. 023115, 2020.
- [29] Y. Chen, F. Meng, Z. Lan, B. Jia, and X. Huang, “Dual-polarization second-order photonic topological insulators,” *Phys. Rev. Appl.*, vol. 15, no. 3, p. 034053, 2021.
- [30] Z. Du, H. Chen, and G. Huang, “Optimal quantum valley Hall insulators by rationally engineering Berry curvature and band structure,” *J. Mech. Phys. Solid.*, vol. 135, p. 103784, 2020.
- [31] J. Luo, Z. Du, L. Chang, M. Yue, W. Zhang, and Xu. Guo, “Moving morphable components-based inverse design formulation for quantum valley/spin Hall insulators,” *Extreme Mech. Lett.*, vol. 45, p. 101276, 2021.
- [32] Xu. Guo, W. Zhang, and W. Zhong, “Doing topology optimization explicitly and geometrically—a new moving morphable components based framework,” *J. Appl. Mech.*, vol. 81, no. 8, p. 081009, 2014.
- [33] R. Xue, L. Chang, W. Zhang, et al., “Explicit structural topology optimization under finite deformation via moving morphable void (MMV) approach,” *Comput. Methods Appl. Mech. Eng.*, vol. 344, pp. 798–818, 2019.
- [34] J. Langbehn, P. Yang, L. Trifunovic, F. von Oppen, and P. W. Brouwer, “Reflection-symmetric second-order topological insulators and superconductors,” *Phys. Rev. Lett.*, vol. 119, no. 24, p. 246401, 2017.
- [35] H. W. Dong, Y. S. Wang, T. X. Ma, and X. X. Su, “Topology optimization of simultaneous photonic and phononic bandgaps and highly effective photonic cavity,” *J. Opt. Soc. Am. B Opt. Phys.*, vol. 31, no. 12, pp. 2946–2955, 2014.
- [36] H. Shin, J. A. Cox, R. Jarecki, A. Starbuck, Z. Wang, and P. T. Rakich, “Control of coherent information via on-chip photonic–phononic emitter–receivers,” *Nat. Commun.*, vol. 6, no. 1, pp. 1–8, 2015.
- [37] J. Jiang, M. Chen, and J. A. Fan, “Deep neural networks for the evaluation and design of photonic devices,” *Nat. Rev. Mater.*, vol. 6, pp. 679–700, 2021.
- [38] L. Yang, J. Ren, and H. Chen, “Unsupervised manifold clustering of topological phononics,” *Phys. Rev. Lett.*, vol. 124, no. 18, p. 185501, 2020.